Natural and forced convection heat transfer coefficients of various finned heat sinks for miniature electronic systems

Article *in* Proceedings of the Institution of Mechanical Engineers Part A Journal of Power and Energy · June 2018

DOI: 10.1177/0957650918784420

CITATIONS
12

READS
6,359

4 authors, including:

Ong kok seng
Universiti Tunku Abdul Rahman
80 PUBLICATIONS **1,951** CITATIONS
SEE PROFILE

Koon Chun Lai
Self Funded
62 PUBLICATIONS **469** CITATIONS
SEE PROFILE

Mohammad Sajad Naghavi
KFM Energy Solutions Sdn Bhd
28 PUBLICATIONS **1,131** CITATIONS
SEE PROFILE

Original Article

Institution of MECHANICAL ENGINEERS
Journal of POWER AND ENERGY

Proc IMechE Part A:
J Power and Energy
0(0) 1–13

DOI: 10.1177/0957650918784420
journals.sagepub.com/home/pia
SAGE

Natural and forced convection heat transfer coefficients of various finned heat sinks for miniature electronic systems

SW Pua[1], KS Ong[1], KC Lai[1] and MS Naghavi[2]

Abstract

Downward lighting light-emitting diodes require cooling with cylindrical fin heat sinks to be mounted on top and cooled under natural convection air cooling mode. Performance simulation would involve specification of the heat transfer coefficient. Numerous methods are available to simulate the performance of conventional plate fin heat sinks including computational fluid dynamics packages. It would be feasible to perform simulation based on conventional flat plate fin heat sinks. A cylindrical fin heat sinks could be simply treated as a plate fin heat sink, if we imagine it cut open and laid out horizontally. A theoretical model is proposed in this paper. An experimental investigation is conducted here to validate its accuracy. Convective heat transfer coefficients were experimentally determined for a horizontally and vertically inclined bare plate operating under natural and forced air cooling modes. In addition, a vertical plate fin heat sink and a vertical cylindrical fin heat sink under natural convection were investigated. Power inputs were kept from 5 to 40 W in order to keep operating temperatures below 100 °C. Comparison of the experimental heat transfer coefficients and those obtained from well-known existing Nusselt number correlations show that agreement was poor for the bare plate but satisfactory for the plate and cylindrical fin heat sinks. Although they are within the generally accepted range, it would be advisable for actual measurements to be carried out in order to provide more accurate sizing for thermal measurements.

Keywords

Heat exchanger, convection heat transfer coefficient, fin heat sink, natural convection, forced convection

Date received: 25 January 2018; accepted: 29 May 2018

Introduction

In recent years, with the emergence of high power electronic devices, thermal management and heat dissipation have become important issues. A bare plate (BP) is commonly employed to provide uniform heat distribution. Based on Newton's law of cooling, heat transfer rate may be increased by increasing the heat transfer coefficient (h), or by increasing the heat transfer surface area. As a consequence, the base-to-environment cooling temperature difference for heat transfer would be reduced. Heat transfer could be also be enhanced by using extended surfaces like attaching fins to a BP to form a plate fin heat sink (PFHS). PFHS is most common because of its inherent simplicity, reliability, and low cost. It could be cooled under natural convection (NC) or forced convection (FC) air cooling mode. In order to determine heat transfer rate from the PFHS, h need to be specified. Most texts state that convective h lie in the range between 2 and 25 W/m^2 K for NC and 25 and 250 W/m^2 K for FC. They would range of values encountered is because they depend upon material, size, and geometrical configuration like fin spacing, thickness, length and shape of the fins, as well as on cooling mode and heat transfer medium.

A conventional PFHS under NC air cooling mode is commonly used in cooling applications due to its simplicity and reliability. Studies on the design

[1]Depatment of Industrial Engineering, Universiti Tunku Abdul Rahman, Malaysia
[2]Real State Division, UEM Edgenta Berhad, Malaysia

Corresponding author:
KS Ong, Depatment of Industrial Engineering, Universiti Tunku Abdul Rahman, Kampar, Perak 31900, Malaysia.
Email: skong@utar.edu.my

of heat sinks under NC have been extensively carried out based on both experimental and numerical methods.[1–9] Starner and McManus[1] reported that the vertically inclined PFHS performed better than the horizontal or 45° inclined ones. Likewise, Guvenc and Yuncu[2] reported that the vertical PFHS performed better than the horizontal base unit. A numerical study of PFHS by Baskaya et al.[3] showed that fin spacing, length, and height significantly affected the overall heat transfer. In particular, Harahap and McManus[4] showed that shorter fin lengths resulted in higher heat transfer. Welling and Wooldridge[5] showed that large fin spacing improved thermal performance due to less inter-fin boundary layer interference. Further, Dayan et al.[6] observed that fin length has greater effect than fin height. Various studies by Huang and Wong[7] and Taji et al.[8] on the PFHS showed that the flow pattern changed from a steady single-chimney to an oscillating sliding-chimney flow, or vice versa, depending on fin length. Pouryoussefi and Zhang[9] investigated the PFHS with circular pins between the rectangular base plates and showed that lower thermal resistance was obtained with the pins.

In dealing with the rapid growth of miniature electronic systems that require drastic heat dissipation, various active methods were introduced to enhance the heat transfer of the PFHS.[10–12] Numerous papers have been written on the thermal performance of PFHS under FC. Iyengar and Bar-Cohen[13] presented a coefficient of performance analysis for the PFHS to optimize the FC cooling that could be achieved in a specified volume with least material and energy consumed. Peles et al.[14] stated that FC was an effective heat transfer mode over the fin heat sinks. In addition, Ong et al.[15] showed that the h values obtained under FC were higher than those under NC.

Recently, cylindrical fin heat sinks (CFHS) consisting of cylindrical cylinders with parallel longitudinal fins are employed for LED down-lighting applications. Haldar et al.[16] showed that fin thickness played the most influential role in the heat transfer rate on the horizontal CFHS. A numerical study by Wu and Tao[17] showed that fin height, fin number, and orientation significantly affected the thermal performance of CFHS. Empirical Nusselt number correlations have been developed for the design of heat sinks during the early stages of thermal design.[18,19] Jang et al.[20] concluded that vertical orientation achieved the highest heat transfer rate as the air flowed upward along the fins. They also concluded that the orientation effect was intensified when the number of fins and the fin length increased, whereas fin height was insignificant. Lee et al.[21] proposed an empirical correlation to estimate the Nusselt number for NC from vertical cylinders with inclined fins. Park et al.[22] proposed an empirical correlation for vertical cylinders with branched fins and showed that branched fins performed better than those of plate fins. Li et al.[23] investigated the performance of CFHS with perforated rings and concluded that the thermal resistance of CFHS with optimized perforated ring was less than that of nonperforated rings by 17%.

Numerous correlations have been proposed by various authors for fin heat sinks for thermal management (cooling and heat spreading) based on dimensionless parameters like Nusselt, Rayleigh, Prandtl, and Reynolds numbers. However, as pointed out by Lewandowski and Kubski[24] they could differ by up to ±50%. Downward lighting with light emitting diodes (LEDs) require them to be cooled with cylindrical fin heat sinks (CFHSs) mounted on the top and are cooled under NC air cooling mode. There are numerous and well-known methods available to simulate the performance of the PFHS. Investigations to determine the h associated with CFHSs are few and far in between. Simulation methods are quite limited although CFD packages are available. It would be feasible to simulate their performances based on PFHSs. A CFHS could be simply treated as a PFHS if we imagine it cut open and laid out horizontally. A theoretical concept model is proposed in this paper. An experimental investigation is conducted here to evaluate its accuracy.

The present investigation would be to determine the experimental values of h and the extent to which they differ from the well-known correlations for the following fin heat sinks:

i. A BP operating under NC and FC air cooling modes and orientated horizontally and vertically.
ii. A vertical PFHS consisting of an array of rectangular fins laid out parallel on a flat base under NC air cooling mode.
iii. A vertical CFHS with an array of rectangular parallel fins arranged radially outwards under NC cooling mode.

Theoretical model

Bare plate

A theoretical model of a BP is presented in Figure 1. Dimensions of the plate with width (W), length (L), plate thickness (Δx_{base}), and thermal conductivity (k_{hs}) is shown in Figure 1(a). Heat transfer (Q) is assumed to be one-dimensional and to be via convection only as radiation heat transfer is expected to be relatively small and is neglected here. The temperature distribution across the plate is shown in Figure 1(b). The surface temperature of the heat source (T_s) is higher than the interface temperature (T_{hs}) between the bottom of the plate and the heat source because of thermal contact resistance (R_{cr}). Convective heat transfer coefficient (h) and temperatures at the heat transfer surface (T_{fm}) and ambient (T_a) are assumed to be uniform. The associated thermal resistance network is shown in Figure 1(c).

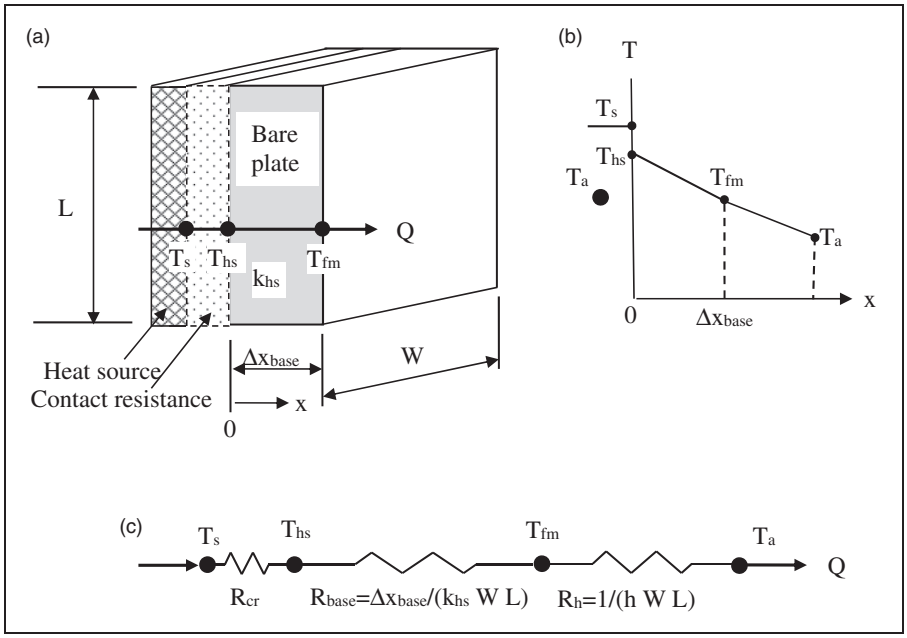

Figure 1. Theoretical model of BP. (a) Isometric view. (b) Temperature distribution across bare plate. (c) Thermal resistance network.

Base and surface convective thermal resistances could be determined from

$$R_{base} = \frac{\Delta x_{base}}{k_{hs}\ W\ L} \tag{1}$$

$$R_h = \frac{1}{h\ W\ L} \tag{2}$$

Hot plates could be cooled by either NC or FC air cooling modes with the plates positioned horizontally or vertically. Under NC, the h would depend to a greater extent on plate orientation than under FC. For horizontal isothermal plate under NC, Incropera et al.[25] recommended

$$Nu_{LC} = 0.54\ Ra_{L_C}^{1/4}\ \left(10^4 \leqslant Ra_{L_C} \leqslant 10^7\right) \tag{3}$$

where the characteristic length (L_C) of the plate is defined by the ratio of total heat transfer area/wetted perimeter

$$L_C = \frac{W\ L}{2\ (W+\ L)} \tag{4}$$

For a vertical plate, Churchill and Chu[26] recommended

$$Nu_L = 0.68 + \frac{0.670\ Ra_L^{1/4}}{\left[1 + (0.492/\ \mathrm{Pr})^{9/16}\right]^{4/9}} \quad Ra_L \leqslant 10^9 \tag{5}$$

Under FC, air flow is normally parallel to and along the plate. As a result, h would be independent of orientation. For isothermal laminar FC flow parallel to a hot plate, Incropera et al.[25] recommended

$$\overline{\mathrm{Nu}_L} = 0.664\ \mathrm{Re}_L{}^{1/2}\ \mathrm{Pr}^{1/3}\ \ (\mathrm{Re}_L \leqslant 5 \times 10^5 \text{ and } \mathrm{Pr} \geqslant 0.6) \tag{6}$$

All fluid properties are evaluated at the film temperature

$$T_f = \frac{(T_{fm} + T_a)}{2} \tag{7}$$

For NC, Lewandowski and Kubski[24] proposed correlations different from the above. For this study, we will only compare the h values obtained from the above Nusselt number correlations.

The interface temperature could be determined from

$$T_{hs} = T_a + Q\ (R_{base} + R_h) \tag{8}$$

Plate fin heat sink

A theoretical model of a PFHS is presented in Figure 2. It comprises a number of straight rectangular profile fins (N_{fin}) with pitch (S_{fin}), fin length (L), fin height (H_{fin}), fin thickness (t_{fin}), and base plate thickness (Δx_{base}) as shown in Figure 2(a). Air flow is assumed to be parallel to the fins. In the vertical orientation, the fins are aligned vertically under NC air cooling mode. Radiation heat transfer is neglected. The temperature distribution across the base of the plate is assumed to be linear, as shown in

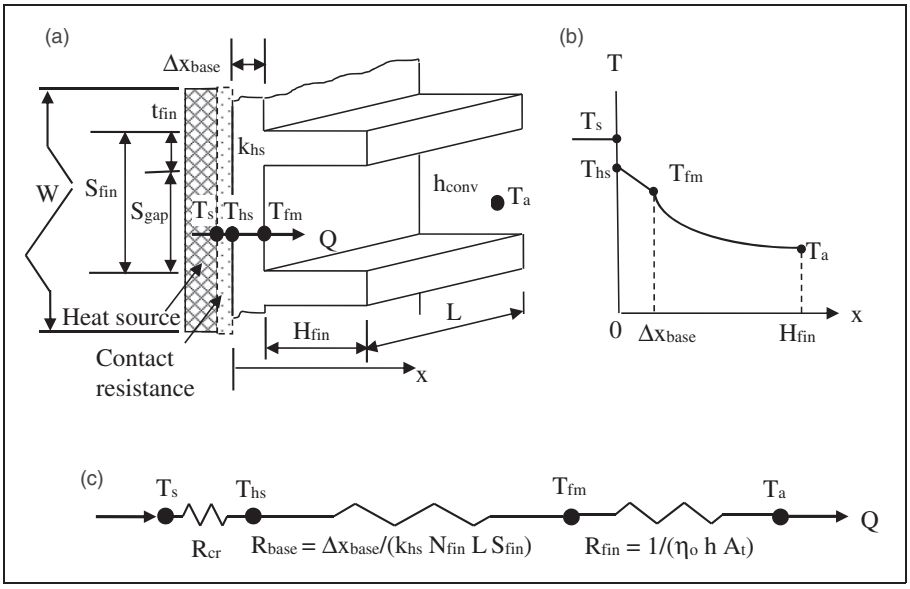

Figure 2. Theoretical model of PFHS with straight rectangular fins. (a) Isometric view. (b) Temperature distribution across fin heat sink. (c) Thermal resistance.

Figure 2(b). The surface temperature of the heat source (T_s) is higher than the bottom surface temperature (T_{hs}) of the PFHS because of thermal contact resistance. Heat transfer is assumed to be one-dimensional at the base and spreads uniformly to the finned and unfinned portions of the PFHS. For simplicity, the entire PFHS is assumed to be at a uniform temperature (T_{fm}).

The total width of the PFHS is calculated from

$$W = N_{fin}\, x\, S_{fin} \tag{9}$$

where N_{fin} is the total number of fins and S_{fin} is the pitch of the fin array.

The distance or gap between fins is given by

$$S_{gap} = S_{fin} - t_{fin} \tag{10}$$

where t_{fin} is the fin thickness.

For a straight fin of uniform cross section and a corrected fin height with an adiabatic tip, the fin efficiency is given by

$$\eta_{fin} = \frac{\tanh\,(m_{fin}\, H_{fin,c})}{(m_{fin}\, H_{fin,c})} \tag{11}$$

where

$$m_{fin} = \sqrt{\frac{2\,(L\, +\, t_{fin})\, h}{L\, t_{fin}\, k_{hs}}} \tag{12}$$

and corrected fin height

$$H_{fin,c} = H_{fin} + \frac{t_{fin}}{2} \tag{13}$$

In an array consisting of a number of fins the total heat transfer surface area of the PFHS is

$$A_t = N_{fin}\,(A_{fin} + A_{fin,b}) \tag{14}$$

where the heat transfer area of each fin

$$A_{fin} = (2\, H_{fin}\, + t_{fin})\, L \tag{15}$$

and the heat transfer area of each nonfinned or bare portion of the array

$$A_{fin,b} = S_{gap}\, L \tag{16}$$

The overall surface fin efficiency of a multi-fin array and the base surface to which they are attached to is given by

$$\eta_o = 1 - \frac{N_{fin}\, A_{fin}}{A_t}(1 - \eta_{fin}) \tag{17}$$

A thermal resistance model of a PFHS is shown in Figure 2(c). Base and fin thermal resistances could be determined from

$$R_{base} = \frac{\Delta x_{base}}{k_{hs}\, N_{fin}\, L\, S_{fin}} \tag{18}$$

$$R_{fin} = \frac{1}{\eta_o\, h\, A_t} \tag{19}$$

The interface temperature could be determined from

$$T_{hs} = T_a\, +\, Q\,(R_{base}\, +\, R_{fin}) \tag{20}$$

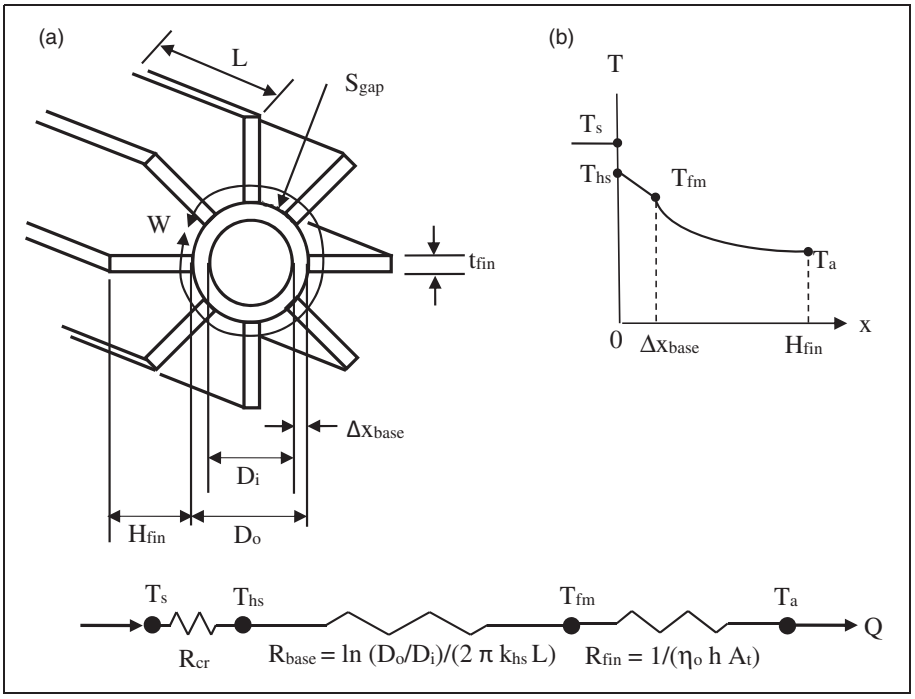

Figure 3. Theoretical model of CFHS with longitudinal fins. (a) Isometric view. (b) Temperature distribution across fin heat sink.

Cylindrical fin heat sinks

A theoretical model of a CFHS is presented in Figure 3. The unit comprises a cylinder with a number of straight rectangular profile fins (N_{fin}) uniformly distributed radially outwards with pitch (S_{gap}), fin length (L), fin height (H_{fin}), and fin thickness (t_{fin}) as shown in Figure 3(a). The CFHS is orientated vertically under NC air cooling mode. Radiation heat loss is neglected. The temperature distribution across the base of the cylinder is assumed linear as shown in Figure 3(b). The surface temperature of the heat source (T_s) is higher than the bottom surface temperature (T_{hs}) of the PFHS because of thermal contact resistance. Heat transfer is assumed to be one-dimensional and spreads uniformly outwards to the finned and unfinned portions of the device. Again, for simplicity, the entire CFHS is assumed to be at a uniform temperature (T_{fm}).

An equivalent average width is given by

$$W = 0.5\,\pi\,(D_o + D_i) \tag{21}$$

The fin pitch on the outer diameter of the cylinder is

$$S_{fin} = \frac{\pi\,D_o}{N_{fin}} \tag{22}$$

S_{gap} is calculated from equation (10).

A thermal resistance model of the CFHS is shown in Figure 3(c). Base thermal resistance is determined from

$$R_{base} = \frac{\ln\,(D_o/D_i)}{2\,\pi\,k_{hs}\,L} \tag{23}$$

R_{fin} is calculated from equation (19) and interface temperature from equation (20).

Experimental investigation

Experimental set-up

Experiments were carried out on the following:

- BP orientated horizontally and vertically and under NC and FC,
- PFHS orientated vertically and under NC,
- CFHS orientated vertically and under NC.

All the devices were fabricated from aluminium. Dimensions of the BP were $W = 99.7$ mm, $L = 99.9$ mm, and $\Delta x_{base} = 5.1$ mm. For the PFHS, $W = 100$ mm, $L = 100$ mm, and $\Delta x_{base} = 5.2$ mm. It had 10 fins with $H_{fin} = 30$ mm and $t_{fin} = 3.5$ mm. The CFHS had the following dimensions: $H_{fin} = 20$ mm, $D_o = 44$ mm, $D_i = 40$ mm, $t_{fin} = 2$ mm, $N_{fin} = 40$, $L_{fin} = 100$ mm, $W_{fin} = 132$ mm, and $S_{fin} = 3$ mm. Experimental set-ups for all the three units are quite similar. Heat was applied via flat rectangular electrical heating elements at the bottom for both the BPHS and the PFHS. For the BP, input power (Q) was set at 5 W, 10 W, and 20 W and controlled to within $\pm$ 0.2 W with an ac voltage regulator. For the PFHS, P_{HS} was set at 10 W, 20 W, and 40 W. For the CFHS, a cartridge type electric heating element supplied heat at 20 W, 40 W, and 60 W. A table fan was employed for FC, producing an air speed of about 1.5–2.0 m/s across the BP and 2.0–3.0 m/s in between the fins for the PFHS. Type T thermocouples

(accuracy $\pm 0.5\,^{\circ}$C) were employed throughout to measure temperatures. All thermocouples were connected to a "Graphtec" data logger and logged every minute. The time taken to reach steady state was about 120 min under NC and about 30 min under FC. Each run was conducted three times to ensure results were repeatable. Generally, temperatures were uniform to within $\pm 0.3\,^{\circ}$C and repeatable to within $0.5\,^{\circ}$C. A thermocouple located nearby measured the ambient temperature (T_a). Laboratory condition was not controlled and ambient temperature varied from about $19\,^{\circ}$C to $22\,^{\circ}$C. Thermocouples (T_{ins}) attached to the external surface of the insulation showed temperature difference between insulation and ambient were less than $2\,^{\circ}$C at low power and $5\,^{\circ}$C at high power. Heat loss was estimated to be less than 5% of the total power input. The estimated error in determining h is about 8% for low power and 6% for high power.

Thermal conductivity of (k_{hs}) of pure aluminum is about 200 W/m^{2}K and for aluminum alloy from 50 to 100 W/m^2 K. With plate dimensions $\Delta x_{base} = 5$ mm, $W = 100$ mm, and $L = 100$ mm, base thermal resistance (R_{base}) varies from 0.01 to 0.003 K/W. A thermal interface material is usually provided to reduce thermal contact resistance (R_{cr}). Manufacturer's data stated that R_{cr} was 0.005 K/W. The thermocouple probes were inserted through the aluminum block and measured the heating surface temperature. Since thermal contact resistance is small, the interface or junction temperature between the heater and the bottom of the aluminum block could be assumed equal to the mean heating surface temperature in all cases.

Figure 4 shows the set up for the BP. The locations of thermocouples are shown in Figure 5. Nine holes drilled from the top of the plate through to its base enabled thermocouples to be inserted to determine the temperature of the heating surface temperature

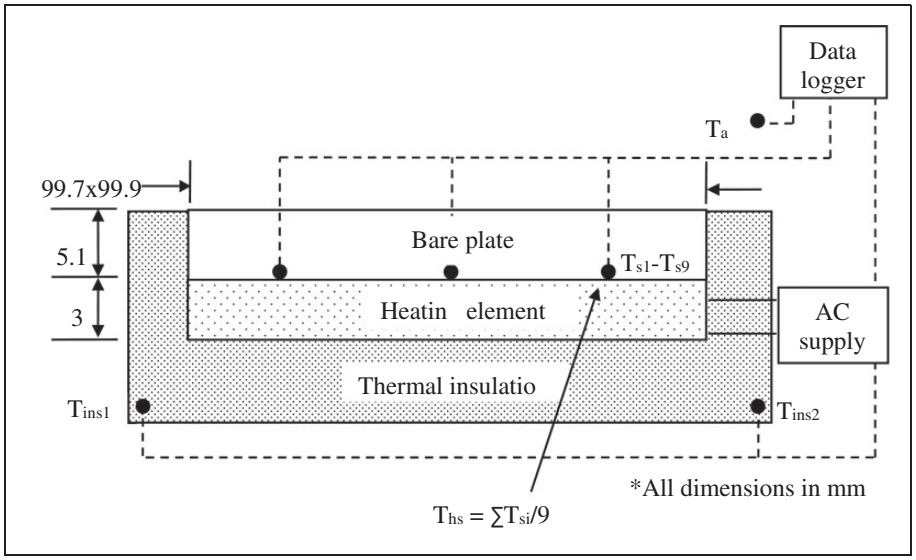

Figure 4. Experimental set-up for BP.

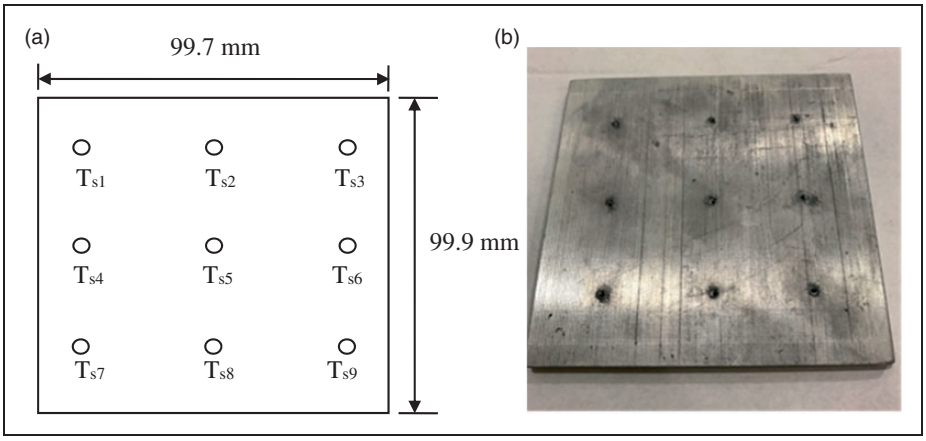

Figure 5. Location of thermocouples in BP.

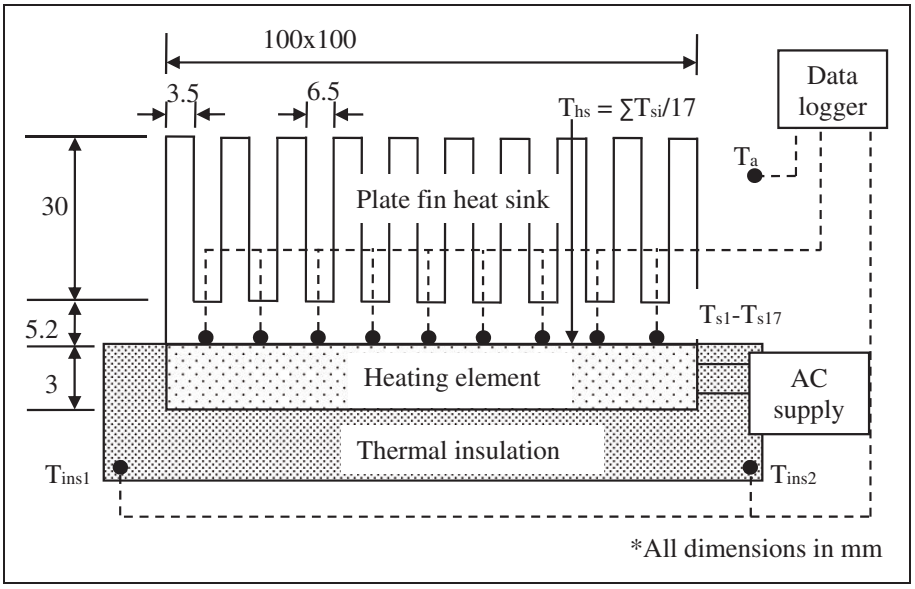

Figure 6. Experimental set-up for PFHS.

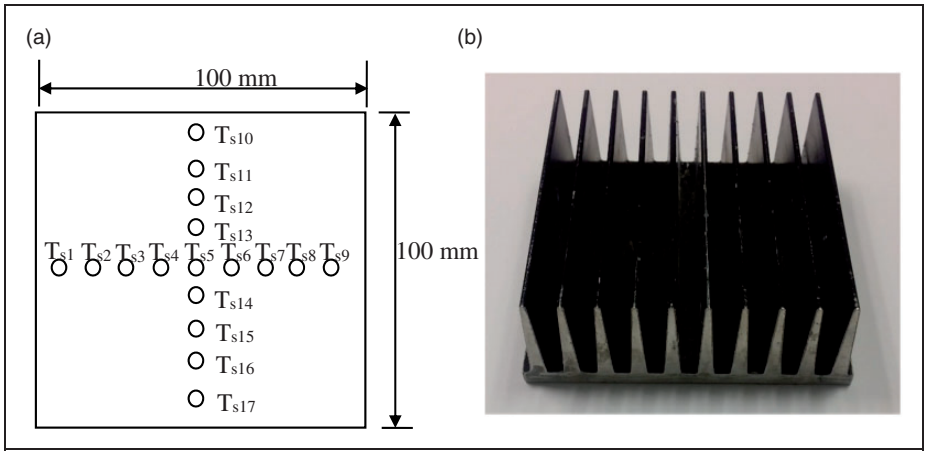

Figure 7. Location of thermocouples in PFHS.

($T_{s1} - T_{s9}$). The experimental set up for the PFHS is shown in Figure 6. Seventeen thermocouple holes ($T_{s1} - T_{s17}$) were drilled at the locations shown in Figure 7. Figure 8 shows the set up for the CFHS with locations of 8 thermocouples (T_{s1-s8}). A photograph of the CFHS is shown in Figure 9.

For each set-up, experimental h values are calculated. For the BP

$$h_{\exp} = (W\,L)^{-1}\left[\frac{(T_{hs} - T_a)}{P_{EH}} - \frac{\Delta x_{base}}{W\,L\,k_{hs}}\right]^{-1} \quad (24)$$

For the PFHS

$$h_{\exp} = \left[\eta_o\,N_{fin}\,L\,(2\,H_{fin} + S_{fin})\right]^{-1} \times \left[\frac{(T_{hs} - T_a)}{P_{EH}} - \frac{\Delta x_{base}}{k_{hs}\,N_{fin}\,L\,S_{fin}}\right]^{-1} \quad (25)$$

and for the CPHS

$$h_{\exp} = \left[\eta_o\,N_{fin}\,L\,(2\,H_{fin} + S_{fin})\right]^{-1} \times \left[\frac{(T_{hs} - T_a)}{P_{EH}} - \frac{\ln(D_o/D_i)}{2\,\pi\,k_{hs}\,L}\right]^{-1} \quad (26)$$

Uncertainty analysis

There can be several factors that may lead to errors, including individual instrument uncertainty, calibration errors, data reduction errors, and data acquisition errors. Thus, an uncertainty analysis was carried out to allocate credible limits to presented results' accuracy, by considering the calibration errors for each of the parameters deemed most effective. The reading of the following parameters is considered to

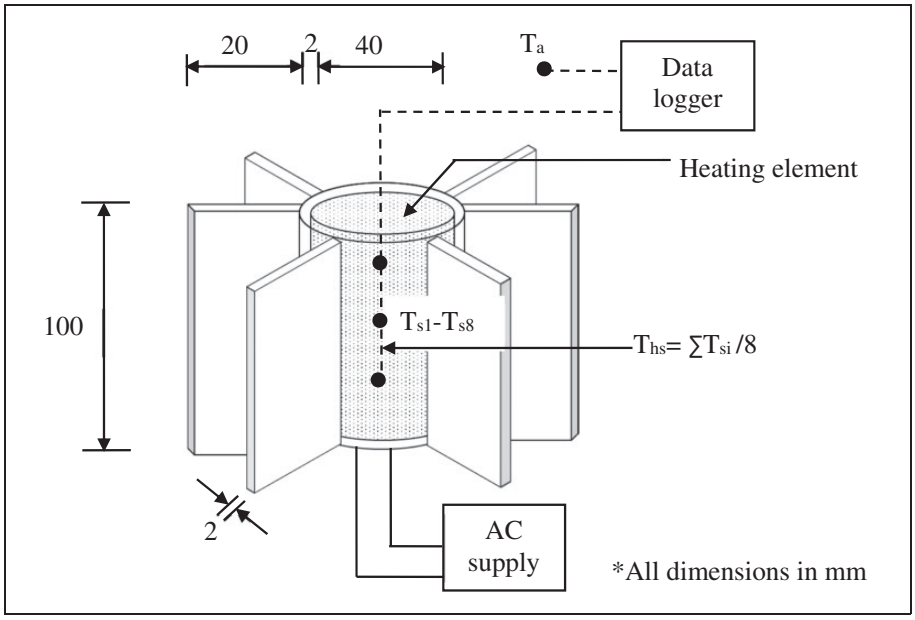

Figure 8. Experimental set-up for CFHS.

Figure 9. Photograph of CFHS.

determine the tests results

$$\eta_w = f(P_{EH}, T_s, T_{hs}, T_{fm}, T_a, L_{fin}, A_{hs})$$

The uncertainty associated with each measurement can be mathematically expressed as

$$\frac{\delta\eta_w}{\eta_w} = \sqrt{\left(\frac{\delta X_1}{X}\right)^2 + \left(\frac{\delta X_2}{X}\right)^2 + \cdots + \left(\frac{\delta X_n}{X}\right)^2}$$

where n is the number of parameters, $\frac{\delta X_1}{X}$ corresponds to the standard uncertainty of the parameters.

Input power (Q) errors is estimated to be about 2% in 10 W input. All the TCs were calibrated and the measured errors of the TCs for heat source, heat sink, fin material, and ambient temperature are ±1.7%, ±1.7%, ±1.5%, and ±1.5%, respectively. Same data for heat sink material and dimensions are ±2% and ±1.4%, respectively. According to these values, by using the equations above, the uncertainty of the overall thermal resistance network expressed in Figures 1 to 3 is determined to be about ±4.5%.

Results and discussion

Experimental results showing temperatures at the heating surface, ambient, and insulation are summarized in Table 1 together with experimental (h_{exp}) and correlated (h_{corr}) values obtained from the Nusselt equations. For simplicity, property values are obtained by assuming fin temperature (T_{fm}) is equal to heating surface temperature (T_{hs}).

Heating surface temperatures

Heater surface temperatures (T_{hs}) are plotted against input heat flux in Figure 10 for all three cases.

All the results show that T_{hs} increases with input power as expected. For the horizontal BP, T_{hs} increased from 49 °C at 500 W/m^2 to 117 °C at 2000 W/m^2 under NC and from 29 °C to 54 °C under FC. For the vertical BP, T_{hs} increased from 49 °C at 500 W/m^2 to 112 °C at 2000 W/m^2 under NC and from 28 °C to 48 °C under FC.

Also, as expected, NC cooling mode results in higher temperatures. For example, at 2000 W/m^2, T_{hs} reached up to 112 °C for the vertical BP under NC cooling mode compared to 48 °C under FC with the same power input.

Table 1. Experimental data for bare plate (BP), plate (PFHS), and cylindrical fin heat sinks (CFHS).

Type	Q (W)	P''_{EH} (W/m^2)	NC/FC	Orientation	T_{ins} (°C)	T_a (°C)	T_{hs} (°C)	h_{exp} (W/m^{2}K)	h_{corr} (W/m^{2}K)
BP	5	500	NC		22.5 ± 0.3	21.0 ± 0.3	49.1 ± 0.5	17.9 ± 0.1	6.7
	10	1000		Horizontal	24.2 ± 0.2	21.3 ± 0.3	73.4 ± 0.2	19.3 ± 0.1	7.7
	20	2000			25.8 ± 0.2	21.1 ± 0.2	116.8 ± 0.5	21.0 ± 0.2	8.8
	5	500			22.8 ± 0.2	21.5 ± 0.6	48.9 ± 0.4	18.4 ± 0.5	4.7
	10	1000		Vertical	24.3 ± 0.3	21.6 ± 0.6	71.6 ± 0.5	20.1 ± 0.4	5.3
	20	2000			26.0 ± 0.1	21.9 ± 0.6	111.9 ± 0.2	22.3 ± 0.1	6.1
	5	500	FC		20.9 ± 0.1	20.2 ± 0.2	28.5 ± 0.2	60.2 ± 0.1	19.5
	10	1000		Horizontal	21.8 ± 0.1	19.9 ± 0.1	37.3 ± 0.1	61.2 ± 0.2	19.5
	20	2000			23.9 ± 0.1	20.8 ± 0.1	54.3 ± 0.4	61.9 ± 0.1	19.5
	5	500			21.4 ± 0.2	21.1 ± 0.4	27.8 ± 0.5	74.7 ± 0.6	19.6
	10	1000		Vertical	22.5 ± 0.3	21.4 ± 0.6	34.8 ± 0.5	74.9 ± 0.6	19.5
	20	2000			23.8 ± 0.2	21.5 ± 1.0	48.1 ± 1.2	75.2 ± 0.6	19.5
	10	1000			22.4 ± 0.2	20.5 ± 0.2	45.3 ± 0.1	5.5 ± 0.1	4.6
PFHS	20	2000	NC	Vertical	24.3 ± 0.2	20.5 ± 0.2	63.2 ± 0.2	6.3 ± 0.1	5.2
	40	4000			26.1 ± 0.1	20.5 ± 0.1	93.9 ± 1.0	7.4 ± 0.1	5.8
	10	758			21.8 ± 0.2	19.3 ± 0.3	41.4 ± 0.3	2.6 ± 0.1	4.4
CFHS	20	1515	NC	Vertical	24.3 ± 0.3	19.1 ± 0.4	58.1 ± 0.1	2.8 ± 0.1	5.1
	40	3030			26.6 ± 0.1	19.0 ± 0.1	85.0 ± 0.3	3.3 ± 0.1	5.7

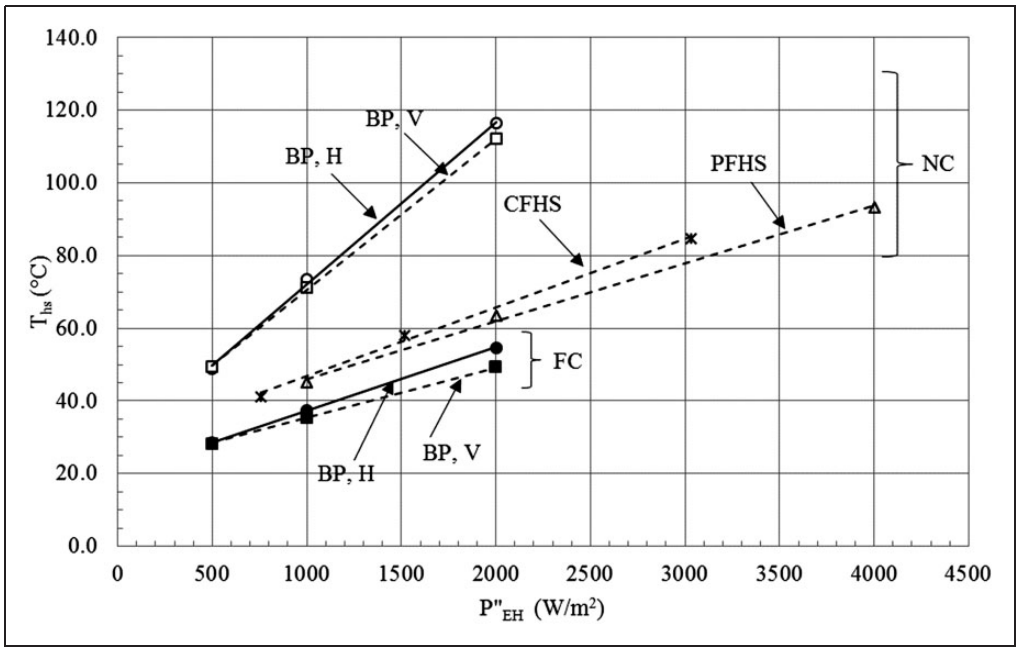

Figure 10. Experimental results of T_{hs}.

Under both NC and FC cooling modes, the surface temperature of the vertical BP plate is about 20 °C lower for the BP at a high heat flux of 2000 W/m^2. At the low heat flux of 500 W/m^2 there is hardly any difference between the two temperatures.

The vertical BP performs slightly better than the horizontal plate at high heat input. For example, under NC, T_{hs} for the vertical BP reached up to 112 °C compared to 117 °C for the horizontal plate at 2000 W/m^2. At the low heat input of 500 W/m^2, there is not much difference between the vertical plate under NC at 49 °C and the horizontal plate under FC at 29 °C.

The three devices are of different sizes. A performance comparison could be attempted in terms of heat flux. Under NC and for vertical inclination, the PFHS shows a lowest surface temperature of 63 °C compared to 58 °C for the CFHS and 112 °C for the BP

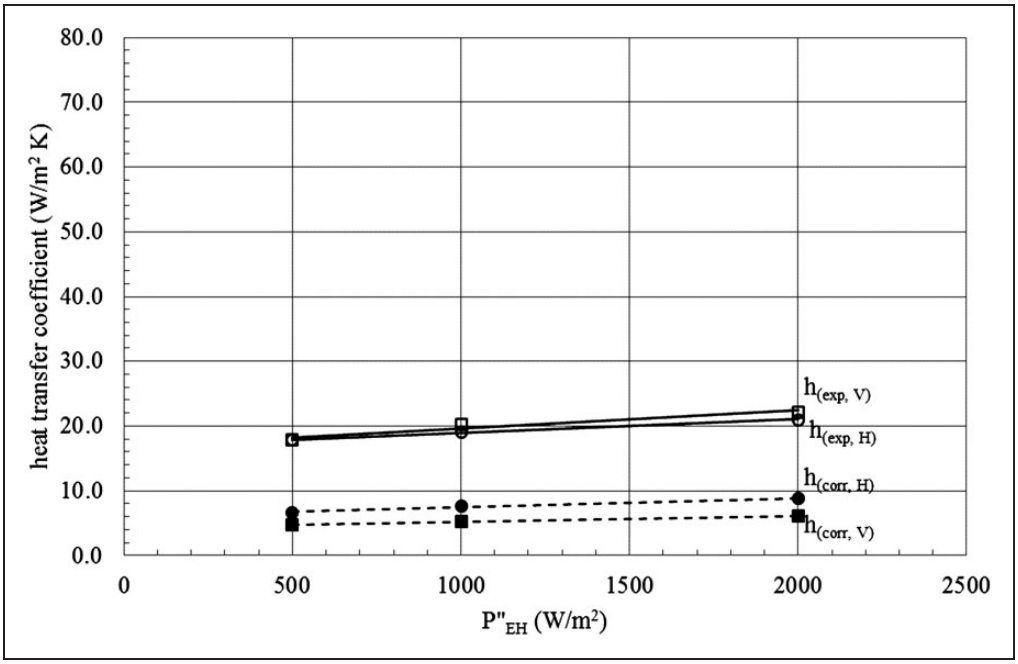

Figure 11. Comparison of experimental and Nusselt number *h* for horizontal and vertical BP under NC.

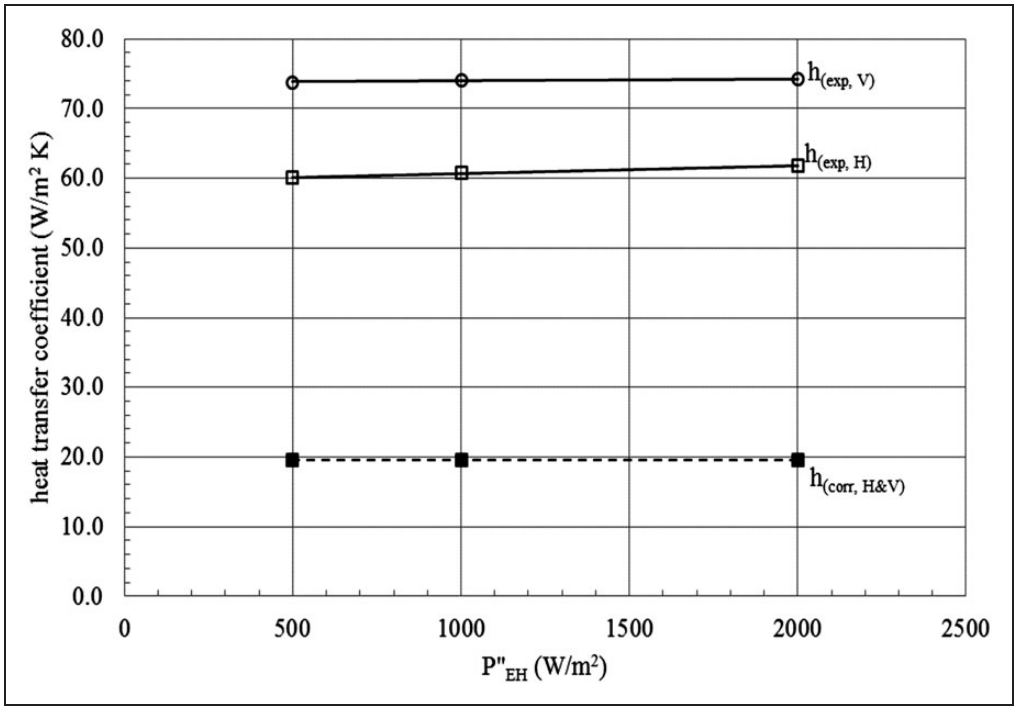

Figure 12. Comparison of experimental and Nusselt number *h* for horizontal and vertical BP under FC.

at 2000 W/m^2. This shows that the PFHS performs best of the three devices under NC cooling mode.

Heat transfer coefficients

Experimental h_{exp} values for the vertical and horizontal BP under NC cooling mode are shown and compared with correlated h_{corr} values in Figure 11. The results show that *h* values increase with power input as expected. For example, under NC, h_{exp} increases from 18.4 W/m^2 K at 500 W/m^2 to 21.0 W/m^2 K at 2000 W/m^2 for the horizontal BP. The effect of plate inclination under NC is small. The difference between the vertical and horizontal plate results at 2000 W/m^2 is only about 1.3 W/m^2 K. Experimental and correlated *h* values for the vertical BP under FC cooling mode are shown and compared in Figure 12. For FC, values are calculated based on an air speed of 2.3 m/s.

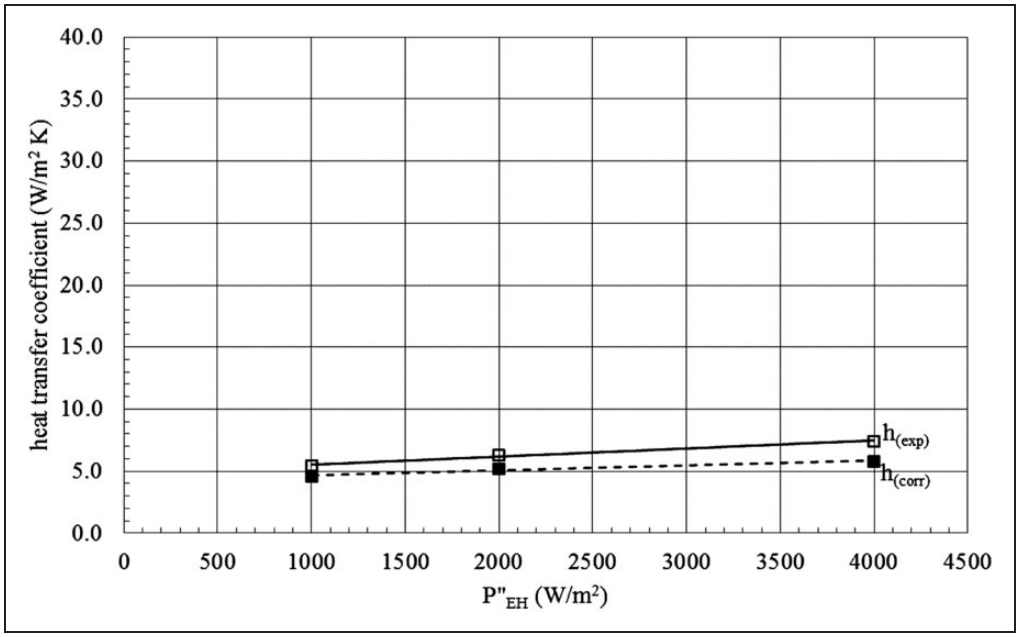

Figure 13. Comparison of experimental and Nusselt number *h* for vertical PFHS under NC.

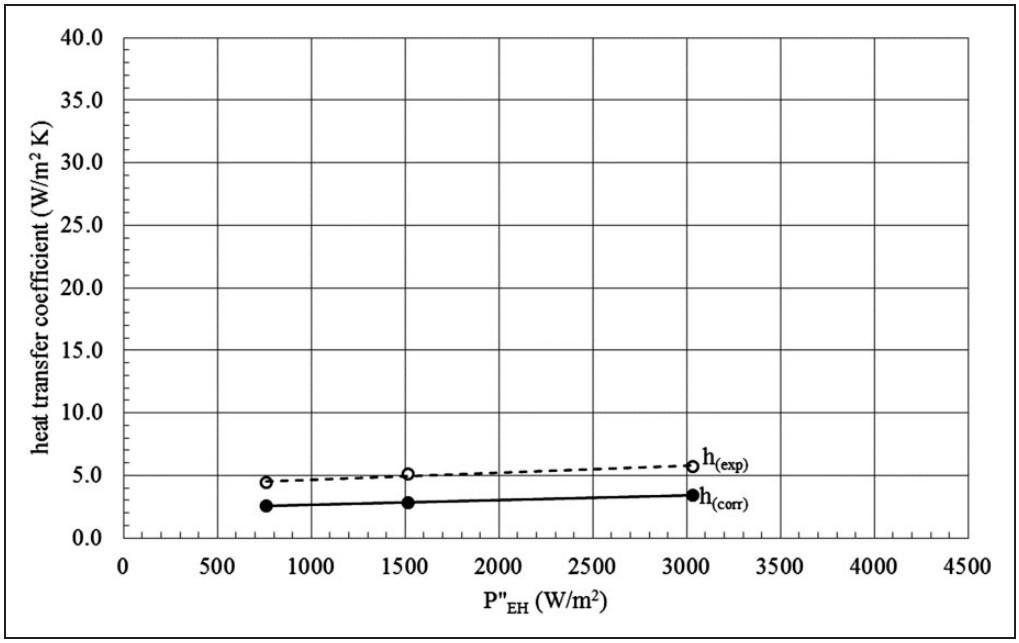

Figure 14. Comparison of experimental and Nusselt number *h* for vertical CFHS under NC.

The results show that h increases from 60.2 to 61.9 W/m^2 K for the horizontal plate and from 74.9 to 75.2 W/m^2 K for the vertical plate under FC. The effect of power input from 500 W/m^2 to 2000 W/m^2 is very small, within 1.7 W/m^2 K for the horizontal plate and 0.5 W/m^2 K for the vertical plate. Experimental h_{exp} are about 3 to 4 times higher than those obtained from correlation under both NC and FC cooling modes for either plate inclinations. Since air flow has been assumed to be parallel to the plate, h_{corr} is not affected by inclination.

Experimental h_{exp} results for the vertical PFHS under NC are shown and compared with correlated h_{corr} results in Figure 13. Experimental h_{exp} increased only from 5.5 W/m^2 K at power input of 500 W/m^2 to 7.4 W/m^2 K at 2000 W/m^2. The increase with power input is quite marginal. Experimental h_{exp} are higher than h_{corr} values by about 20%. For example, h_{exp} varied from 5.5 to 7.4 W/m^2 K while h_{corr} varied from 4.6 to 5.8 W/m^2 K.

Results for the vertical CFHS under NC are shown and compared in Figure 14. Experimental h_{exp}

increased marginally from 2.6 W/m^2 K at power input of 500 W/m^2 to 3.3 W/m^2 K at 2000 W/m^2. Experimental h_{exp} are higher than h_{corr} values by about 50%. For example, h_{exp} varied from 2.6 to 3.3 W/m^2 K while h_{corr} varied from 4.4 to 5.7 W/m^2 K.

Convective h depends upon material, surface finish, ambient, and heated surface temperature conditions. Under NC cooling mode, plate inclination also affect its performance. Under FC, plate inclination would not have much effect as air flow is normally parallel to the plate. Lasance[27] showed that there was a 100% variation in published results for the correlations. The present investigation for the BP showed that h depended upon orientation and air cooling modes. For the BP we have shown that h depended upon both orientation and cooling mode. Generally, they are expected to lie in the range of 2–25 W/m^2 K for NC and 25–250 W/m^2 K for FC. The results show that although experimental values are higher than those obtained from the correlations, they are within the accepted range.

Conclusions

Convective h was experimentally determined for a horizontal and vertical BP under both NC and FC air cooling modes, a vertical PFHS under NC mode and a vertical CFHS under NC mode. Power inputs were kept around 5–40 W in order to keep operating temperatures below 100 °C.

The following conclusions could be made:

1. Heating surface temperature increased with input power as expected.
2. NC cooling mode resulted in higher surface temperatures.
3. Surface temperature of the vertical BP is lower than for the horizontal plate at high heat flux.
4. At low heat input, there is not much difference between the surface temperatures of the vertical and horizontal BPs.
5. The PFHS performs best of the three devices udner NC cooling mode.
6. Experimental h are higher than those obtained from the correlations.

Comparison of the experimental h values with those obtained from generally accepted Nusselt number correlations show that agreement was poor for the horizontal and vertical BP under NC and FC but satisfactorily for the vertical PFHS and CFHS under NC. However, they are within the generally accepted range of values. Nonetheless, it would be advisable for actual measurements to be made in order to provide more accurate sizing for precise thermal management.

Declaration of Conflicting Interests

The author(s) declared no potential conflicts of interest with respect to the research, authorship, and/or publication of this article.

Funding

The author(s) disclosed receipt of the following financial support for the research, authorship, and/or publication of this article: This study was funded by the University Internal Fund (UTARRF) under project IPSR/RMC/UTARRF/2015-C2/O02.

References

1. Starner KE and McManus HN. An experimental investigation of free convection heat transfer from rectangular fin arrays. *J Heat Transfer* 1963; 85: 273–278.
2. Guvenc A and Yuncu H. An experimental investigation on performance of fins on a horizontal base in free convection heat transfer. *Heat Mass Transfer* 2001; 37: 409–416.
3. Baskaya S, Sivrioglu M and Ozek M. Parametric study of natural convection heat transfer from horizontal rectangular fin array. *Int J Therm Sci* 2000; 39: 797–805.
4. Harahap F and McManus HN. Natural convection heat transfer from horizontal rectangular fin arrays. *J Heat Transfer* 1967; 89: 32–38.
5. Welling JR and Wooldridge CB. Free convection heat transfer coefficients from rectangular vertical fins. *J Heat Transfer* 1965; 87: 439–444.
6. Dayan A, Kushnir R, Mittelman G, et al. Laminar free convection underneath a downward facing hot fin array. *Int J Heat Mass Transfer* 2004; 47: 2849–2860.
7. Huang GJ and Wong SC. Dynamic characteristics of natural convection from horizontal rectangular fin arrays. *Appl Therm Eng* 2012; 42: 81–89.
8. Taji SG, Parishwad GV and Sane NK. Experimental investigation of heat transfer and flow pattern from heated horizontal rectangular fin array under natural convection. *Heat Mass Transfer* 2014; 50: 1005–1015.
9. Pouryoussefi SM and Zhang Y. Experimental study of air-cooled parallel plate fin heat sinks with and without circular pin fins between the plate fins. *J Appl Fluid Mech* 2015; 8: 515–520.
10. Lai K, Tan C, Ong K, et al. Thermal field simulation of multi package LED module. In: *IEEE international symposium on next-generation electronics (ISNE)*, Taipei, Taiwan, 2015, pp.1–3.
11. Khan NS, Gul T, Islam S, et al. Magnetohydrodynamic nanoliquid thin film sprayed on a stretching cylinder with heat transfer. *Appl Sci* 2017; 7: 271.
12. Sathyabhama A and Dinesh A. Augmentation of heat transfer coefficient in pool boiling using compound enhancement techniques. *Appl Therm Eng* 2017; 119: 176–188.
13. Iyengar M and Bar-Cohen A. Least-energy optimization of forced convection plate-fin heat sinks. *IEEE T Compon Pack Technol* 2003; 26: 62–70.
14. Peles Y, Koşar A, Mishra C, et al. Forced convective heat transfer across a pin fin micro heat sink. *Int J Heat Mass Transfer* 2005; 48: 3615–3627.
15. Ong KS, Tan CF, Lai KC, et al. Heat spreading and heat transfer coefficient with fin heat sink. *Appl Therm Eng* 2017; 112: 1638–1647.
16. Haldar SC, Kochhar GS, Manohar K, et al. Numerical study of laminar free convection about a horizontal cylinder with longitudinal fins of finite thickness. *Int J Therm Sci* 2007; 46: 692–698.

17. Wu JM and Tao WQ. Numerical computation of laminar natural convection heat transfer around a horizontal compound tube with external longitudinal fins. *Heat Transfer Eng* 2007; 28: 93–102.
18. An BH, Kim HJ and Kim DK. Nusselt number correlation for natural convection from vertical cylinders with vertically oriented plate fins. *Exp Therm Fluid Sci* 2012; 41: 59–66.
19. Kim HJ, An BH, Park J, et al. Experimental study on natural convection heat transfer from horizontal cylinders with longitudinal plate fins. *J Mech Sci Technol* 2013; 27: 593–599.
20. Jang D, Park SJ, Yook SJ, et al. The orientation effect for cylindrical heat sinks with application to LED light bulbs. *Int J Heat Mass Transfer* 2014; 71: 496–502.
21. Lee JB, Kim HJ and Kim DK. Experimental study of natural convection cooling of vertical cylinders with inclined plate fins. *Energies* 2016; 9: 391.
22. Park KT, Kim HJ and Kim DK. Experimental study of natural convection from vertical cylinders with branched fins. *Exp Therm Fluid Sci* 2014; 54: 29–37.
23. Li B, Jeon S and Byon C. Investigation of natural convection heat transfer around a radial heat sink with a perforated ring. *Int J Heat Mass Transfer* 2016; 97: 705–711.
24. Lewandowski WM and Kubski P. Methodological investigation of free convection from vertical and horizontal plates. *Warme Stoffubertragung* 1983; 17: 147–154.
25. Incropera FP, Dewitt DP, Bergman TL, et al. *Fundamentals of heat and mass transfer*. 6th ed. New York: Wiley, 2011.
26. Churchill SW and Chu HHS. Correlating equations for laminar and turbulent free convection from a horizontal cylinder. *Int J Heat Mass Transfer* 1975; 18: 1323–1329.
27. Lasance CJM. Sense and nonsense of heat transfer correlations applied to electronics cooling. In: *6th international conference on thermal, mechanical and multiphysics simulation and experiments in micro-electronics and microsystems, EuroSimE*, Berlin, Germany, 18–20 April 2005.

Appendix

Notation

A	heat transfer area (m^2)
c_p	specific heat (J/kg K)
D	external diameter (m)
g	gravitational accereration (m/s^2)
Gr	Grashoff number
h	convection heat transfer coefficient (W/m^2 K)
H	fin height (m)
$H_{fin,c}$	corrected fin height (m)
k	thermal conductivity of heat sink (W/m K)
L	length (m)
L_C	characteristic length (m)
m_{fin}	fin parameter
N	number
Nu	Nusselt number ($= \frac{h L}{k}$)
Q	power input (W)
P''_{EH}	heat flux (W/m^2)
Pr	Prandtl number ($= \frac{c_p \mu}{k}$)
R	thermal resistance
R_h	convection thermal resistance (K/W)
R_{cr}	thermal contact resistance (K/W)
Ra	Rayleigh number ($= Gr\ \mathrm{Pr} = \frac{g \beta (T_s - T_\infty) L^3}{\nu \alpha}$)
Re	Reynolds number ($= \frac{\rho u D}{\mu}$)
S_{gap}	fin gap (m)
S_{fin}	fin pitch (m)
t	thickness (m)
T	temperature (°C, K)
T_{fm}	fin temperature (°C, K)
u	velocity (m/s)
W	width (m)
Δx_{base}	thickness of heat sink base (m)
β	coefficient of expansion of air (1/K)
η	efficiency
η_o	overall fin efficiency
μ	dynamic viscosity of air (kg/m s)
ν	kinematic viscosity of air (m^2/s)
π	Pi
ρ	density of air (kg/m^3)

Subscripts

a	ambient
base	heat sink base
corr	correlation
exp	experimental
f	fluid properties
fin	fin
fin,b	unfinned
hs	heat sink
i	internal
o	external
s	heat source surface
t	total